Molecular and Cellular Pathobiology

Lysophosphatidic Acid Receptor LPAR6 Supports the Tumorigenicity of Hepatocellular Carcinoma

Antonio Mazzocca[1,2], Francesco Dituri[3], Flavia De Santis[4], Addolorata Filannino[3], Chiara Lopane[1], Regina C. Betz[5], Ying-Yi Li[6], Naofumi Mukaida[7], Peter Winter[8], Cosimo Tortorella[1], Gianluigi Giannelli[9], and Carlo Sabbà[1]

Abstract

The aberrant processes driving hepatocellular carcinoma (HCC) are not fully understood. Lysophosphatidic acid receptors (LPAR) are commonly overexpressed in HCC, but their contributions to malignant development are not well established. In this report, we show that aberrant expression of LPAR6 sustains tumorigenesis and growth of HCC. Overexpression of LPAR6 in HCC specimens associated with poor survival in a cohort of 128 patients with HCC. We took a genetic approach to elucidate how LPAR6 sustains the HCC tumorigenic process, including through an expression profiling analysis to identify genes under the control of LPAR6. RNAi-mediated attenuation of LPAR6 impaired HCC tumorigenicity in tumor xenograft assays. Expression profiling and mechanistic analyses identified Pim-3 as a pathophysiologically relevant LPAR6 target gene. In nonmalignant cells where LPAR6 overexpression was sufficient to drive malignant character, Pim-3 was upregulated at the level of transcription initiation through a STAT3-dependent mechanism. A further analysis of HCC clinical specimens validated the connection between overexpression of LPAR6 and Pim-3, high proliferation rates, and poorer survival outcomes. Together, our findings establish LPAR6 as an important theranostic target in HCC tumorigenesis. *Cancer Res; 75(3); 1–12. ©2014 AACR.*

Introduction

Hepatocellular carcinoma (HCC) is a very frequent malignancy, being the sixth most common cancer worldwide (1). In addition, the incidence of HCC has been increasing over the last years, especially in western countries (2). The etiology of HCC is multifactorial, and the disease is very often preceded by other conditions, including chronic inflammation, liver fibrosis, and cirrhosis, that are frequently associated with hepatitis B virus or hepatitis C virus infection, carcinogen/toxin exposure including alcohol and aflatoxin; gender and metabolic conditions are other risk factors (3, 4). Given the multifactorial etiology of HCC, a better understanding of the common molecular pathogenic mechanisms underlying the tumorigenic process of this disease is essential to help identify more effective therapeutic targets. In this context, different molecular mechanisms driving the process evolving from chronic inflammation and cirrhosis to the formation of dysplastic nodules have been identified (5). These mechanisms may not only involve hepatocytes but also liver microenvironment elements, which contribute to HCC growth and progression (6–8). The HCC microenvironment is considered as a metastasis-promoting element in itself, and although the presence of distant metastases in HCC is rarely observed, intrahepatic metastases are very frequent, being a clear sign of tumor progression and an adverse prognostic factor. Although different mechanisms and predisposing factors for the development of intrahepatic metastases have been investigated (9, 10), intrahepatic metastasis remains a serious clinical problem and the main cause of HCC recurrence.

Lysophosphatidic acid (LPA) receptors are G protein–coupled receptors (GPCR) that bind the bioactive phospholipid LPA and activate multiple cellular responses, including cell proliferation, cytoskeletal rearrangements, motility, and apoptosis (11–13). At least five LPAR (LPAR1-5) are relatively well characterized and currently under investigation (14). LPAR6 is a newly identified receptor, originally referred to as purinergic receptor P2Y5 that has been involved in inherited forms of hair loss, specifically hypotrichosis simplex (15) and woolly hair (16). However, other than these reports, the role of LPAR6 in human disease including cancer has not been investigated. Here, we show that LPAR6 is essential for maintaining the proliferation capacity and the tumorigenic phenotype of HCC, and that the tumorigenicity control exerted by LPAR6 occurs through the transcriptional activation of proto-oncogene *Pim-3*. This mechanism sustains HCC growth and progression.

[1]Interdisciplinary Department of Medicine, University of Bari School of Medicine, Bari, Italy. [2]IRCCS "S. de Bellis", National Institute for Digestive Diseases, Bari, Italy. [3]Department of Emergency and Organ Transplantation, Section of Internal Medicine, Allergology and Clinical Immunology, University of Bari School of Medicine, Bari, Italy. [4]Institut Curie, Centre de Recherche, Pole de Biologie du Développement et Cancer, Paris, France. [5]Institute of Human Genetics, University of Bonn, Bonn, Germany. [6]Cancer Research Institute, Fudan University Shanghai Cancer Center, Shanghai, China. [7]Division of Molecular Bioregulation, Cancer Research Institute, Kanazawa University, Kanazawa, Japan. [8]GenXPro GmbH, Altenhöferallee 3, Frankfurt Main, Germany. [9]Department of Biomedical Sciences and Human Oncology, University of Bari School of Medicine, Bari, Italy.

Note: Supplementary data for this article are available at Cancer Research Online (http://cancerres.aacrjournals.org/).

G. Giannelli and C. Sabbà contributed equally to this article.

Corresponding Author: Antonio Mazzocca, University of Bari School of Medicine, Piazza G. Cesare 11, 70124 Bari, Italy. Phone: 39-080-5593-593; Fax: 39-080-5478-126; E-mail: a.mazzocca@intmed.uniba.it

Materials and Methods

Cells and cell culture conditions

Human HCC cell lines, Huh7, PLC/PRF/5, and HLE and were maintained in DMEM supplemented with 10% bovine calf serum (Gibco; Life Technology), as previously reported (17).

Transfection and lentiviral transduction

Cultured Huh7 were infected by the lentiviral particles, containing 3 target-specific constructs that encode 19–25 nt (plus hairpin) shRNA designed to knock down LPAR6 gene expression and isolated by puromycin selection to obtain clonal propagation. Clones LPAR6-shRNA#8 and LPAR6-shRNA#9 showing a significant silencing of LPAR6 gene were selected and used for further experiments. Control-shRNA lentiviral particles encoding a scrambled shRNA sequence that will not induce specific degradation of any known cellular mRNA were used as negative control. To generate human HCC cell lines stably expressing the LPAR6 gene, 1×10^5 HLE cells per 24-mm dish were transfected with 2 μg of pcDNA 3.1/V5-His-LPAR6, mutants pcDNA 3.1/V5-His-Gln 155X, and pcDNA 3.1/V5-His-Lys125AsnfsX37 or pcDNA 3.1/V5-His-neo as negative control using TransIT-LT1 Transfection Reagent (Mirus) according to the manufacturer's instructions. Selection of transfectant clones was carried out by adding 300 μg/mL of neomycin (G418) to the culture medium.

Cell proliferation

Briefly, 1×10^4 cells were plated onto 24-well plates and allowed to grow up to 5 days in the presence of 10% FBS. At each time points, cells were manually counted using Bürker chamber. All experiments were performed in triplicate, and the viable cells were determined by vital dye.

Quantitative real-time PCR

Total RNA was isolated using the RNeasy Mini Kit (Qiagen) and underwent DNAse treatment (TURBO DNA-free Ambion). Reverse transcription (RT) was then carried out with random primers using 1 μg of total RNA from each sample. Quantitative RT-PCR was performed using predesigned primers and SYBR Green Master Mix (Bio-Rad). Housekeeping Glyceraldehyde 3-phosphate dehydrogenase gene (GAPDH) was used as endogenous control. The following primers were obtained from Integrated DNA Technologies: LPAR6: forward: 5′- TTT GCA CTG GCG TGT GGT T-3′, reverse: 5′-TCT GAG GCA TTG TTA CCC TGA-3′; Ki-67, forward: 5′-TTT CAT TTT ACA GGG CTG TTG ATG-3′, reverse: 5′-GGA GGG TTG TGT AGA AGT GGT GTT-3′; Pim-3, forward: 5′-TCA GTA CCT GTG TTT GTG TGA ATG C-3′, reverse: 5′-CCA GAC ATC TCA CTT TTG AAC TGA A-3′; GAPDH, forward: 5′-CCA CAT CGC TCA GAC ACC AT-3′, reverse: 5′-GCG CCC AAT ACG ACC AAA T-3′.

Colony formation assay

Cells (1×10^5) in culture medium were mixed with a volume of 0.5% top agar twice higher and seeded in 60-mm plates onto a base layer of complete medium containing 0.5% agar in the presence of culture medium. The cells were incubated at 37°C in 5% CO2 in air. After 3 weeks, the number and the size of the colonies were counted and statistically analyzed.

Promoter assays and luciferase experiments

The pGL4.10 (luc2) firefly luciferase reporter gene vectors (Promega) harboring the promoter of the human Pim-3 gene or the deleted mutants of the Pim-3 promoter were generated as previously described (18). For luciferase assays, HLE-LPAR6 or HLE-neo cells were transfected in 96-well plates with the same amount (0.1 μg) of pGL4 vectors containing deleted mutants (p809-luc, p264-luc, and p104-luc) or the entire Pim-3 promoter fragment (p2074-luc) using the TransIT-LT1 Transfection Reagent (Mirus), according to the manufacturer's instructions. Luciferase activities were measured 24 hours after transfection using a dual-luciferase reporter assay kit (Promega). Values are expressed as fold increase in luciferase activities compared with pGL4 empty vector control. All experiments were performed in triplicate.
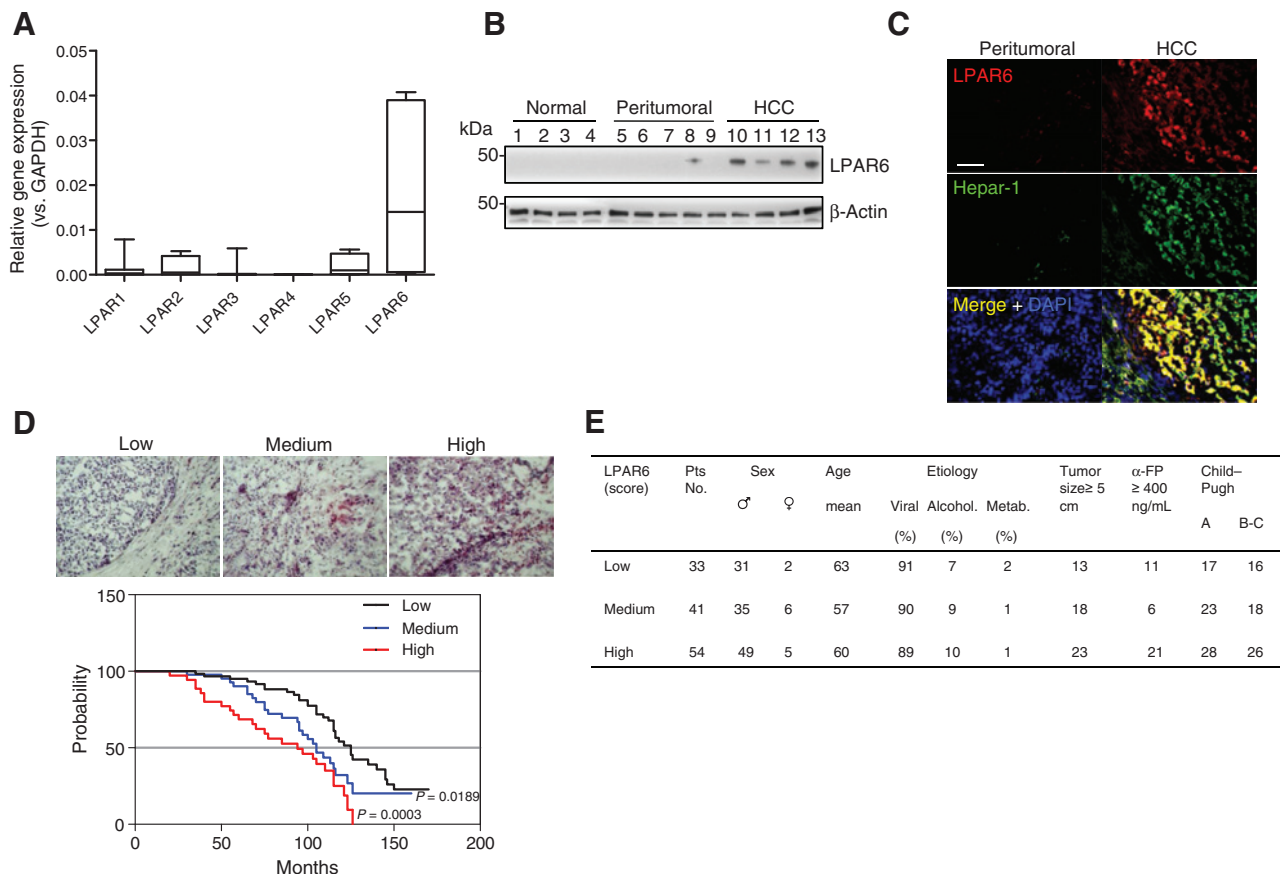
Animal models and *in vivo* procedures

All animal procedures were conducted in accordance with the national and international Guidelines for the Care and Use of Laboratory and were approved by the local Institutional Animal Care and Use Committee. For the evaluation of tumorigenicity after subcutaneous implantation, 4- to 5-week-old female CD-1 nude (nu/nu) athymic mice were subdivided into four groups. The mice were housed and received food and water *ad libitum*. Huh7 parental cells, control-shRNA, LPAR6-shRNA#8, and LPAR6-shRNA#9 from mid-log phase cultures were trypsinized, counted, and then resuspended in a 50% mixture of Matrigel (BD Biosciences) in PBS. A 0.2 mL volume of the cell suspension containing 5.0×10^6 cells/mouse was injected s.c. in the right flank of each mouse. Tumor dimensions and body weights were recorded twice weekly. Tumor sizes (mm^3) were calculated using the equation $(w^2 \times l)/2$, where "w" and "l" refer to the width (mm) and length (mm) recorded at each measurement. For intrasplenic injection, 6-weeks-old male CD-1 nu/nu mice were subdivided into two groups, anesthetized by intraperitoneal injection of a mix of ketamine:xylasine (100:10 mg/kg) diluted in isotonic saline, and then splenically injected with 2×10^6 HLE-LPA cells or HLE-neo in control mice using a 27-gauge needle. The spleen was removed 1 minute after injection and the wound closed using silk suture and surgical clips. Neoplastic progression was monitored based on the general health of the animals. Necropsies were carried out, and snap-frozen liver tumor samples were collected and sectioned at 5 μm for immunohistochemical and hematoxylin and eosin staining, or at 20 μm for RNA extraction.

Massive analysis of cDNA ends for simultaneous gene expression profiling

RNA was extracted from cells and retro-transcribed into cDNA. The population of cDNAs was then bound to a streptavidin matrix via 3′-biotin shred to 50 to 500 bp fragments, and unbound fragments were discarded. The bound fragments were sequenced by next generation sequencing, starting at the fragmentation site, generating 50 to 500 bp "tags." Tags were assembled into contigs and all tags annotated to database entries and counted and finally SNPs were identified. The ToppCluster multiple gene analyzer (Division of Biomedical Informatics, Cincinnati Children's Hospital Medical Center, Cincinnati, OH) was used to group the most significant genes according to their functions using Bonferroni correction and the Kamada–Kawai algorithm and the STRING (Search Tool for the Retrieval of Interacting Genes/Proteins) Database to predict protein interactions.

Liver tissue samples, immunostaining, and immunohistochemical analysis

Samples of HCC tissues were obtained from 128 patients undergoing hepatic resection and classified according to the

Figure 1.
Increased expression levels of LPAR6 in human HCC are correlated with a worse clinical outcome. A, real-time PCR of LPAR6 mRNA expression in patients with HCC ($n = 35$). B, immunoblotting of LPAR6 protein expression in normal liver, peritumoral, and HCC tissues; β-actin is shown as loading control. C, immunofluorescence images showing the colocalization (merge) of LPAR6 (red) and the hepatocyte marker Hepar-1 (green) in HCC tissues compared with peritumoral tissues. Nuclei were stained with DAPI. Scale bar, 100 μm. D, LPAR6 expression levels in representative HCC tissues with different expression levels and score (low, moderate, and high) and Kaplan–Meier plot of overall survival of 68 patients with HCC. Log-rank test shows statistically significant differences between groups (high, $P = 0.0005$; medium, $P = 0.0682$). E, clinical features of the patients subjected to survival analysis.

World Health Organization guidelines. Approval for the study was gained from the local ethics committee, and patients gave prior written informed consent to the use of their tissues. Immunohistochemistry and immunofluorescence were performed as previously described (2). For immunofluorescence analysis, cells or tissue sections were fixed with 4% paraformaldehyde and blocked with 1% BSA/PBS-T. Immunostaining was performed using the appropriate primary and secondary antibodies, and images were acquired using a Nikon eclipse E1000 microscope. For immunohistochemical analysis, frozen liver sections (8 μm) were fixed in acetone-chloroform for 10 minutes and incubated for 1 hour with a polyclonal antibody to LPAR6 (MBL International), and the binding was detected using the APAAP Kit (Dako). Slides were examined under a Nikon eclipse E1000 microscope. Tissues were quantitatively scored according to the percentage of positive cells and staining intensity.

Statistical analyses

The Kaplan–Meier method was used to estimate survival curves, and the log-rank test to test for differences between curves using Prism 5 (Graphpad Software, Inc.). For correlations, Pearson r coefficients were calculated. Data are represented as the mean ± SEM. Significant differences between groups were determined via unpaired two-way or one-way Student t test or ANOVA. $P < 0.05$ was considered statistically significant.

Results

Overexpression of LPAR6 in human HCC is associated with a worse clinical outcome

We examined mRNA expression levels of all known LPAR (LPAR1-6) in human HCC surgical specimens by real-time PCR. Among the six receptors investigated, LPAR6 was the isoform consistently most commonly expressed in analyzed tumor tissues ($n = 35$; Fig. 1A). We next confirmed the presence of elevated protein levels of LPAR6 in the same tissues by Western blotting. Interestingly, the LPAR6 protein was rarely expressed in paired peritumoral tissues and absent in normal control tissues (Fig. 1B). To evaluate the tissue distribution of LPAR6 protein, double immunofluorescence staining was done. This analysis revealed that LPAR6 is expressed by epithelial cancer cells in HCC, as

shown by the colocalization with the hepatocyte marker Hepar-1, whereas no LPAR6 protein expression was detected in paired peritumoral tissues (Fig. 1C). mRNA expression levels of other LPAR (LPAR1-5) in peritumoral tissues are also shown (Supplementary Fig. S1A). Because LPAR6 is present in HCC tissues with different levels of expression, we stratified 128 patients according to their expression levels of LPAR6. Tissues were scored on the basis of the intensity of LPAR6 staining (low, medium, and high), and Kaplan–Meier survival analysis was performed. A significantly longer survival was shown in patients with lower LPAR6 expression levels ($P < 0.001$; Fig. 1D), indicating that expression levels of tumor-associated LPAR6 affect the clinical outcome in patients with HCC. Clinical characteristics of patients included in the survival analysis are shown in Fig. 1E.

LPAR6 sustains growth and tumorigenicity of HCC

We next investigated whether LPAR6 overexpression was relevant to the pathogenesis of HCC, hypothesizing a role of this receptor in controlling tumor proliferation and the tumorigenic phenotype. To gain insight into the mechanism by which LPAR6 regulates growth and tumorigenicity, we used both *in vitro* and *in vivo* approaches. Firstly, we screened five different human HCC cells lines for the expression of both LPAR6 mRNA and protein, and found that HuH7 expressed the highest levels of LPAR6 (Fig. 2A and B). Expression levels of others LPAR (LPAR1-5) are also shown (Supplementary Fig. S1B). Next, we generated stable knocked down LPAR6 in HuH7 using lentiviral delivery of short hairpin RNAs and selected two different cell populations, namely LPAR6-shRNA#8 and LPAR6-shRNA#9, in
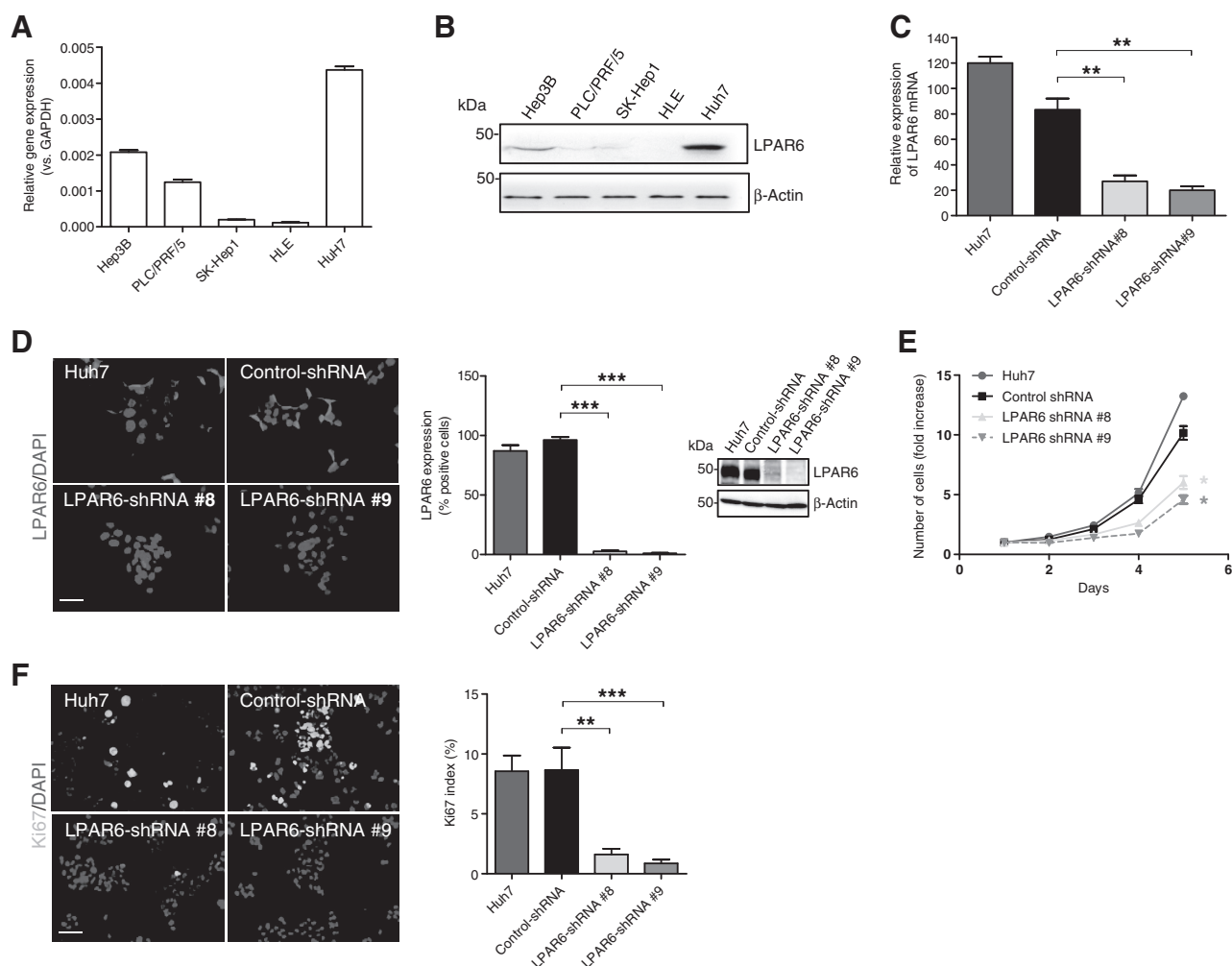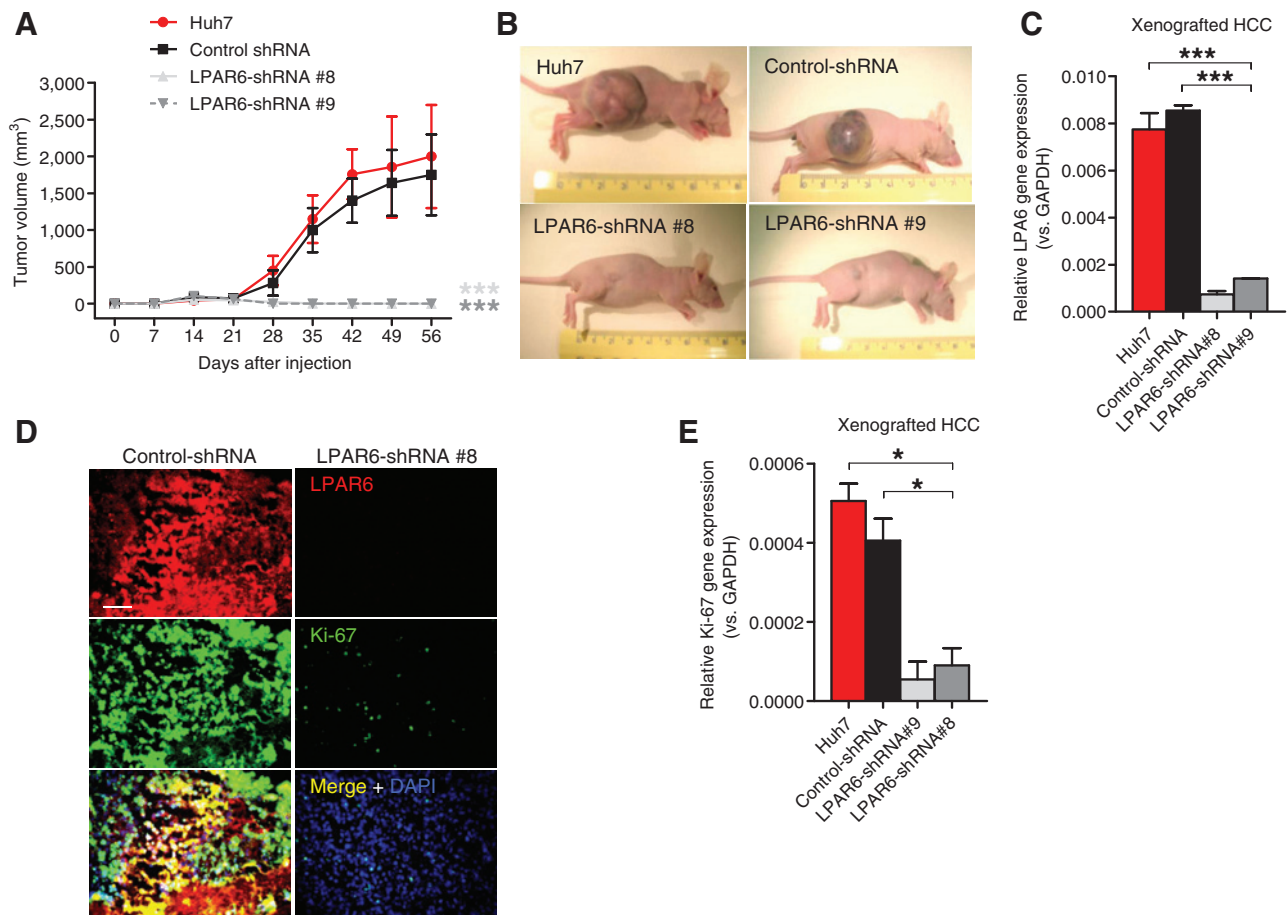

Figure 2.
LPAR6 expression knockdown arrests cell proliferation in HCC. A, LPAR6 mRNA expression levels by real-time PCR analysis in different HCC cell lines (Hep3B, PLC/PRF/5, SK-Hep1, HLE, and Huh7). B, immunoblotting of LPAR6 protein expression in different HCC cell lines (Hep3B, PLC/PRF/5, SK-Hep1, HLE, and Huh7). C, decreased LPAR6 expression determined by real-time PCR in two different populations of LPAR6-silenced cells by shRNA-lentiviral vector (LPAR6-shRNA#8 and LPAR6-shRNA#9) compared with scrambled control (control-shRNA) and the parental cell line Huh7. Error bars, SEM of three independent experiments. **, $P < 0.01$. D, LPAR6 immunofluorescence staining (left) in LPAR6-silenced cells compared with controls and quantitative analysis of LPAR6- stained cells (middle) and Western blot (right) showing a significantly decreased expression of LPAR6 in LPAR6-shRNA#8 and LPAR6-shRNA#9–expressing cells compared with controls. Error bars, SEM of three independent experiments. ***, $P < 0.001$. Scale bar, 100 μm. E, effect of LPAR6-shRNA on Huh7 proliferation compared with controls evaluated by cell counts at different intervals of time. *, $P < 0.05$. Scale bar, 100 μm. F, reduction of the proliferation marker Ki-67 in LPAR6-silenced cells compared with controls. The Ki-67 labeling index shows the significantly reduced percentage of Ki-67–positive cells in LPAR6-silenced cells compared with controls (parental cell line Huh7 and control-shRNA). Error bars, SEM of three independent experiments. **, $P < 0.01$; ***, $P < 0.001$.
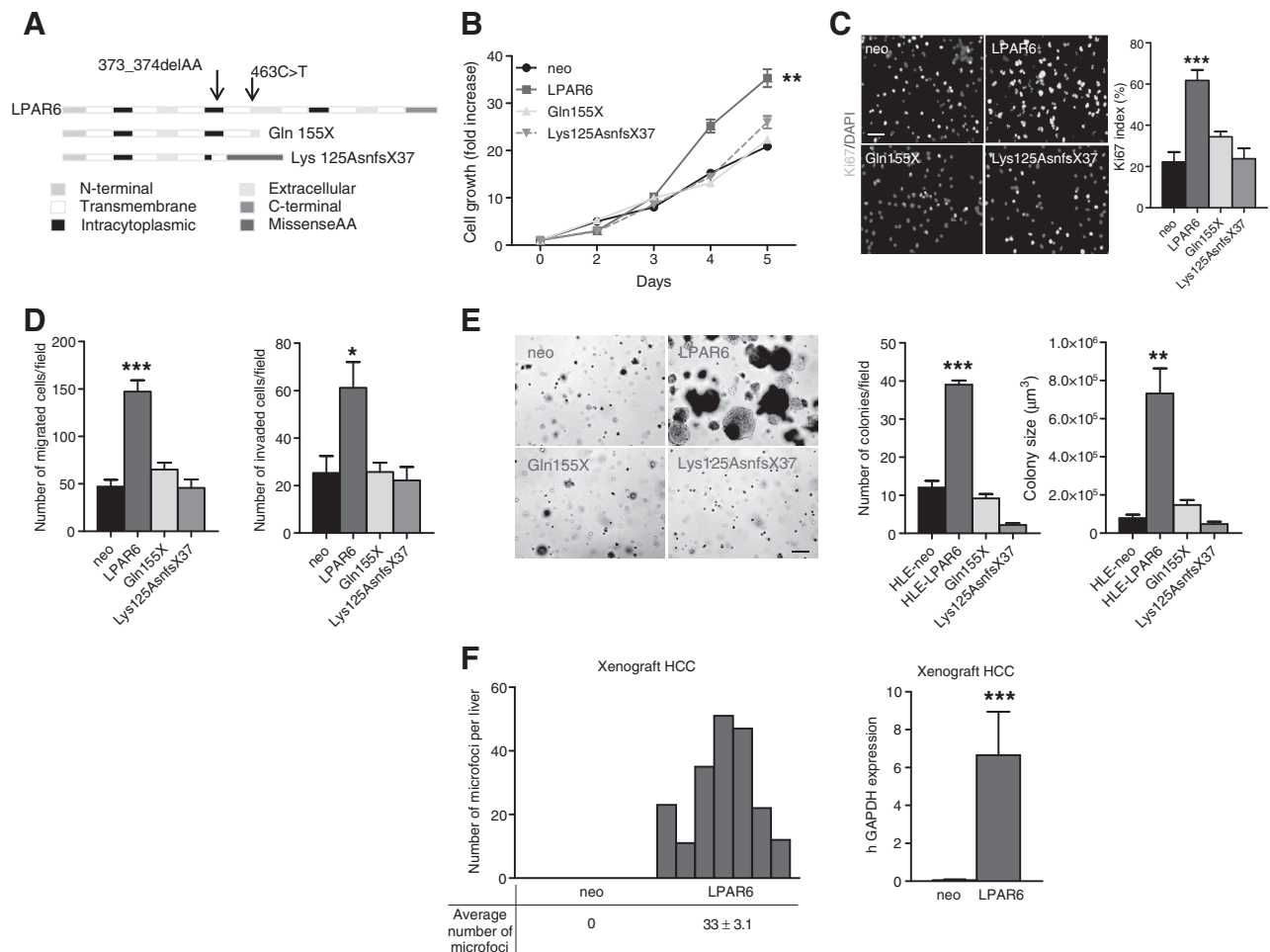
Figure 3.
LPAR6 expression knockdown abolishes the tumorigenicity of HCC cells *in vivo*. A, significant abolishment of tumor growth in nude mice injected with LPAR6-silenced cells (*P* < 0.0001) compared with those injected with control cells (parental cell line Huh7 and control-shRNA). Each data point represents the mean value ± SEM ***, *P* < 0.001. B, representative photographs of nude mice injected with LPAR6-shRNA#8 cells (*n* = 12) or LPAR6-shRNA#9 (*n* = 12) compared with control mice (*n* = 24). C, persistent abolishment of LPAR6 expression in xenografted tumors after tumor excision evaluated by real-time PCR analysis. Error bars, SEM of three independent experiments. ***, *P* < 0.001. D, immunofluorescence staining of LPAR6 and Ki-67 in LPAR6-shRNA tumors compared with controls. Scale bar, 100 μm. E, quantitative PCR analysis showing the significant reduction of Ki-67 in LPAR6-shRNA tumors compared with controls after tumor removal. Error bars, SEM of three independent experiments. *, *P* < 0.05.

which LPAR6 was significantly knocked down (Fig. 2C and D). We then performed five-day proliferation assays and found that LPAR6 knockdown significantly decreased cell growth (*P* < 0.05) in LPAR6-shRNA#8 and LPAR6-shRNA#9 cells as compared with control-shRNA and the parental cell line Huh7 (Fig. 2E). This result was corroborated by a reduced percentage of Ki-67–positive cells (Fig. 2F). Consistently, both LPAR6-shRNA cell populations showed a delayed cell-cycle progression, with a higher percentage of cells in phase G_0–G1 as compared with controls (Supplementary Fig. S2A–S2C), but with no effect on apoptosis (Supplementary Fig. S3A and S3B). To further characterize the LPAR6-knockdown phenotype, we performed Matrigel migration assays that demonstrated a significantly decreased migration of LPAR6-shRNA cells (*P* < 0.001) compared with controls (Supplementary Fig. S4A). We also noticed differences in cell morphology on Matrigel (i.e., a rounded morphology, loss of filopodia and lamellipodia) between LPAR6-shRNA cells and controls (Supplementary Fig. S4B). In addition, the distribution of cortical actin was dramatically

decreased (*P* < 0.001) in both LPAR6-shRNA populations as shown in Supplementary Fig. S4C and quantified in Supplementary Fig. S4D. Finally, no difference in the number of cells adherent to Matrigel was observed (Supplementary Fig. S4E and S4F). Overall, these data indicate that LPAR6 gene knockdown impairs the proliferation ability and tumorigenic phenotype of HCC cells.

To assess the contribution of the LPAR6 to tumor growth and tumorigenicity *in vivo*, we developed a human HCC xenograft model. Four groups of 12 4-week-old female CD-1 nude (nu/nu) athymic mice were formed, and each group was injected with LPAR6-shRNA#8 Huh7 or LPAR6-shRNA#9 Huh7, control-shRNA Huh7, or the parental cell line Huh7. After 8 weeks, mice inoculated with LPAR6-shRNA#8 (*n* = 12) and LPAR6-shRNA#9 (*n* = 12) displayed no significant tumor formation, or very few, small tumors (2 of 24), whereas mice inoculated with control cells all developed (100%) sizeable tumors (mean volume ±SD 1,897.13 ± 10.31 mm³; Fig. 3A and B). To validate the persistence of gene silencing, after sacrifice we checked the expression of

Figure 4.
LPAR6 ectopic expression confers tumorigenic properties to HCC cells. A, schematic illustration of the LPAR6 protein domains wild-type and truncated mutants (p.Gln155X and p.Lys125AsnfsX37); arrows, positions of the mutations c.463C4T and c.373_374delAA. B, increased proliferation of HLE stably transfected with LPAR6 wild type (HLE-LPAR6) compared with the control vector (HLE-neo) and the truncated mutants p.Gln155X and p.Lys125AsnfsX37 evaluated by cell counts at different intervals of time. **, $P < 0.01$ vs. control. C, evaluation of Ki-67 labeling index by immunostaining assay in HLE-LPAR6, HLE-neo, and in the truncated mutants p.Gln155X and p.Lys125AsnfsX37. Scale bar, 100 μm. D, collagen migration and Matrigel invasion assays in HLE-LPAR6, HLE-neo, and the truncated mutants p.Gln155X and p.Lys125AsnfsX37. Error bars, SEM of three independent experiments, each conducted in triplicate. *, $P < 0.05$; ***, $P < 0.001$. E, colony formation assay in HLE-LPAR6, HLE-neo, and the truncated mutants p.Gln155X and p.Lys125AsnfsX37. Error bars, SEM of three independent experiments, each conducted in triplicate. **, $P < 0.01$; ***, $P < 0.001$. F, plot showing the number of microfoci that formed in the liver of athymic CD-1 nu/nu mice 68 days after the intrasplenic injection of HLE-LPAR6 ($n = 6$) or HLE-neo control cells, and mean values for each group (left). Detection of human HCC xenotransplanted cells injected intrasplenically in athymic CD-1 nu/nu mice. After 68 days, mice were sacrificed, and hepatic tissues from HLE-LPAR6 ($n = 10$) and HLE-neo ($n = 10$) injected mice were processed and analyzed by real-time PCR using human-specific GAPDH primers to detect human cancer cells (right). Data, mean ± SEM of three independent experiments, each conducted in triplicate. ***, $P < 0.001$.

LPAR6 in the HCC xenografts and found that LPAR6 expression was still undetectable in LPAR6-shRNA tumors (Fig. 3C). In addition, the Ki-67 proliferative index was markedly reduced in these tumors ($P < 0.05$) compared with controls (Fig. 3D and E), indicating that LPAR6 knockdown reduces tumor growth *in vivo*.

To mirror the tumorigenicity loss induced by LPAR6 knockdown, we next stably overexpressed LPAR6 in HLE cells (hereafter named HLE-LPAR6), an HCC cell line that does not express this receptor (Fig. 2A and B). As control, we generated HLE transfectants expressing the empty vector harboring the neomycin resistance gene (HLE-neo). Expression of LPAR6 in HLE-LPAR6 and HLE-neo was confirmed by real-time PCR and immunoblotting (Supplementary Fig. S5A and S5B). We also

generated HLE expressing two different mutated forms of the LPAR6 gene, mutant c.463C>T, and mutant c.373_374delAA, encoding for the truncated nonfunctional protein p.X and p.Lys125AsnfsX37, respectively (Fig. 4A). Proliferation assays showed that LPAR6 overexpression efficiently increased proliferation in HLE-LPAR6 ($P < 0.01$) compared with HLE-neo. By contrast, increased proliferation was not observed in HLE harboring the truncated mutants Gln155X and HLE-Lys125AsnfsX37, indicating that LPAR6 is indeed required for proliferation (Fig. 4B). Consistently, the number of Ki-67–positive cells was significantly higher in HLE-LPAR6 ($P = 0.0005$) compared with control and LPAR6 truncated mutants (Fig. 4C). We also observed that HLE-LPAR6 cells migrated and

invaded more efficiently compared with HLE-neo, whereas the mutants HLE-Gln155X and HLE-Lys125AsnfsX37 failed to increase migration and invasion (Fig. 4D). Finally, HLE-LPAR6 formed a significantly larger number and size of colonies in soft agar cells compared with HLE-neo and with HLE-Gln155X and HLE-Lys125AsnfsX37 truncated mutants (Fig. 4E). To further validate the effects of LPAR6 on tumorigenesis, we performed *in vivo* experiments. HLE cells are normally non-tumorigenic in mice. To see whether the ectopic expression of LPAR6 confers the ability to form tumors *in vivo*, we carried out experiments in nude mice adopting two different injection methods of HLE-LPAR6 cells, namely subcutaneous and intrasplenic injection. After subcutaneous injection of HLE-LPAR6, few mice (4 of 20) showed a tumor burden and this was not statistically significant (data not shown). By contrast, after intrasplenic injection, although no macroscopic tumors were visible in the liver, we detected the presence of liver neoplastic microfoci in mice injected with HLE-LPAR6, whereas no neo-plastic cells foci were detected in the HLE-neo control group (Fig. 4F, left). This prompted us to further investigate the capacity of HLE-LPAR6 to survive and generate hepatic tumor microfoci. By real-time PCR using human-specific GAPDH primers, we found that HLE-LPAR6 cells were present and surviving in the liver 68 days after injection, whereas no tumors were detected in control mice (Fig. 4F, right). Overall, these data indicate that nontumorigenic HCC cells expressing LPAR6 acquire tumorigenic properties and generate tumor microfoci or can survive in the liver in a dormant state for prolonged periods of time.

The knockdown of LPAR6 affects genes conferring tumorigenic properties

To identify candidate genes under the control of LPAR6, we analyzed transcriptome modifications in LPAR6-silenced HuH7 cells. Gene expression levels were measured by sequencing and counting a single tag originating from the 3' end of mRNAs, a region with a high density of sequence polymorphisms. Using unique molecule identifiers (TrueQuant technique, GenXPro-GmbH), PCR copies were eliminated from the dataset to reduce false-positive SNPs and biased expression values. When compared with regular RNA-seq, the focus on this 3'-untranslated region increases the coverage by 10- to 20-fold and allows a reliable identification of SNPs at comparably lower sequencing costs (Supplementary Fig. S6A). The full list of up- and downregulated genes is reported in Supplementary Tables S1 and S2, respectively. The gene-related function and the network between the most significant up- and downregulated genes in LPAR6-silenced HuH7 cells, analyzed by the STRING database, are summarized in Supplementary Fig. S6B and S6C. Next, the 500 most significant up- and downregulated genes were grouped according to their functions (analysis for comparative cellular processes) using the publicly available software ToppCluster multiple gene analyzer. This analysis revealed that these genes fall into specific categories of function, including cytoskeleton, extracellular matrix (ECM) components, and tissue development (Supplementary Table S3). Because genes regulating tissue development are relevant to carcinogenesis, we focused on this category of genes and in particular on the proto-oncogene Pim-3 as a potential mediator of LPAR6-mediated tumorigenesis (Supplementary Fig. S6D and Supplementary Table S3).
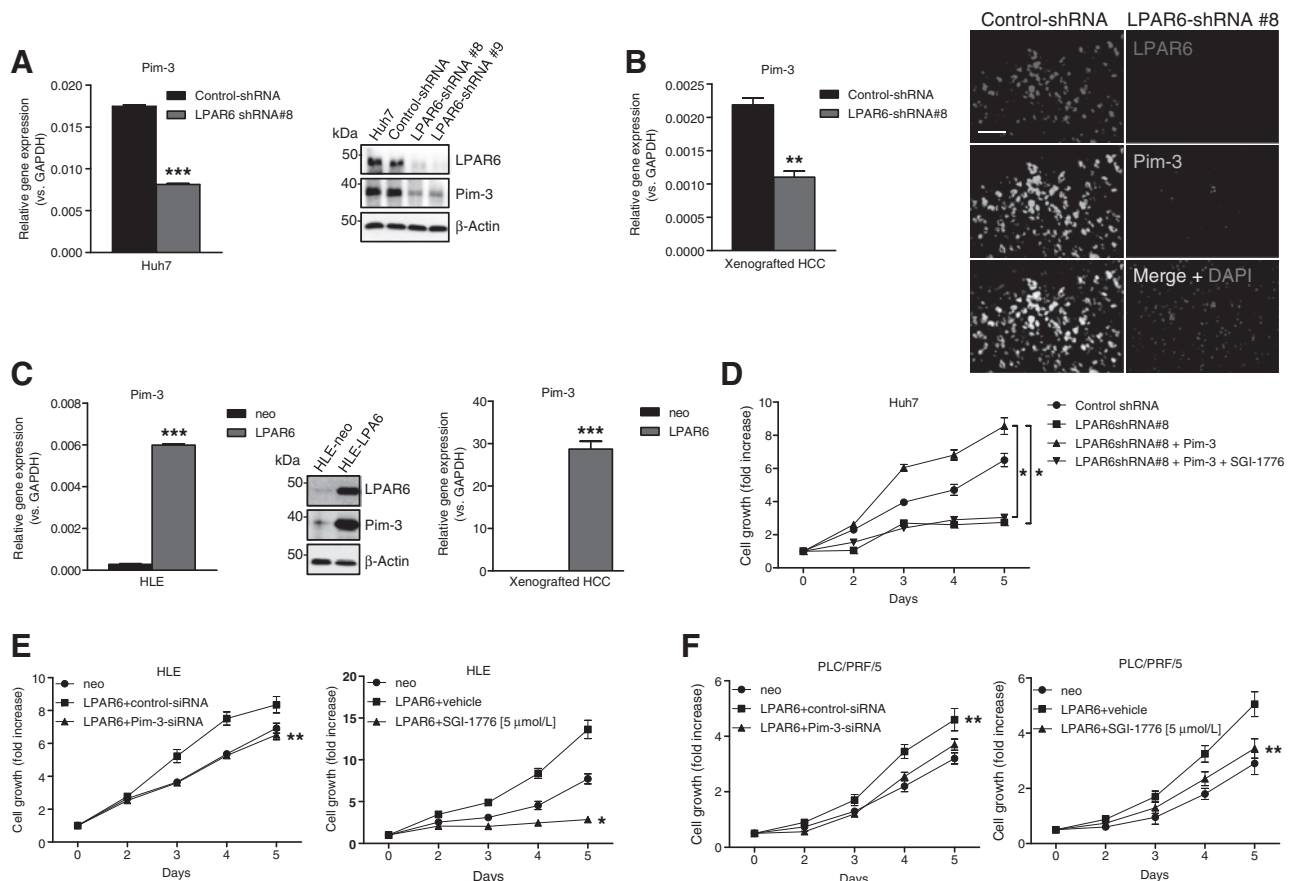
The proto-oncogene *Pim-3* contributes to LPAR6-mediated growth and tumorigenicity

To corroborate the molecular cross-talk between LPAR6 and Pim-3, we measured the mRNA expression levels of Pim-3 in LPAR6–knocked down Huh7 cells and found that Pim-3 was significantly downregulated ($P < 0.001$) in these cells compared with control-shRNA (Fig. 5A). Similarly, the expression levels of both Pim-3 mRNA and protein were significantly decreased ($P < 0.01$) in tumors originated from nude mice inoculated with LPAR6-shRNA HuH7 cells compared with controls (Fig. 5B). Consistently, Pim-3 mRNA levels were upregulated in HLE-LPAR6 cells compared with HLE-neo control cells ($P < 0.001$) and in mice xenotransplanted with HLE-LPAR6 compared with those (control group) transplanted with HLE-neo (Fig. 5C). These findings strongly suggest that Pim-3 is an important contributor to LPAR6-mediated tumor growth.

To validate the direct contribution of Pim-3 to LPAR6-mediated cell growth, we applied our gain- and loss-of-function model. Firstly, we transfected LPAR6-shRNA Huh7 cells with a construct expressing PIM3-GFP and found that ectopic expression of PIM3 completely restored growth in these cells. Then, we treated the same cells with 5 μmol/L of SGI-1776, a pharmacologic PIM3 inhibitor, and observed that PIM3 failed to restore cell growth (Fig. 5D). The effect of SGI-1776 alone on tumor growth *in vivo* (subcutaneous and intrasplenic HCC xenografts) and *in vitro* (LPAR6-expressing HLE) is shown in Supplementary Fig. S7A–S7C. Lastly, we found that inhibition of Pim-3 by both siRNAs and SGI-1776 decreased cell proliferation in HLE-LPAR6 and PLC/PRF/5-LPAR6, two different cell lines overexpressing LPAR6 (Fig. 5E and F). These data confirm the contribution of PIM3 to LPAR6-induced cell proliferation. Finally, we determined whether a correlation between expression of LPAR6 and Pim-3 was detectable in our cohort of patients with HCC, whose clinical and pathologic characteristics are reported in Fig. 1E. We stratified and scored the intensity of LPAR6 staining as high- ($n = 37$) or low-LPAR6 ($n = 33$) expression. Representative immunofluorescence images are shown in Fig. 6A. We found elevated PIM3 tissue expression levels in patients with high levels of LPAR6 ($P < 0.01$; Fig. 6B) and a significant correlation between LPAR6 and PIM3 in these patients ($P < 0.0001$; $R = 0.55$; Fig. 6C). We also sought to determine the correlation between LPAR6 expression and the proliferative marker Ki-67 by measuring stained areas of tissues. We detected elevated Ki-67 levels in high-LPAR6 tissues and low levels of Ki-67 in low-LPAR6 tissues ($P < 0.001$; Fig. 6D and E). A Pearson scatterplot showing the significant correlation ($P = 0.0002$; $R = 0.54$) between Ki-67 and LPAR6 is shown in Fig. 6F. This positive correlation between LPAR6 and Pim-3 expression and with the proliferative marker Ki-67 in patients with HCC is consistent with our findings showing a contribution of PIM3 to LPAR6-induced cell proliferation.

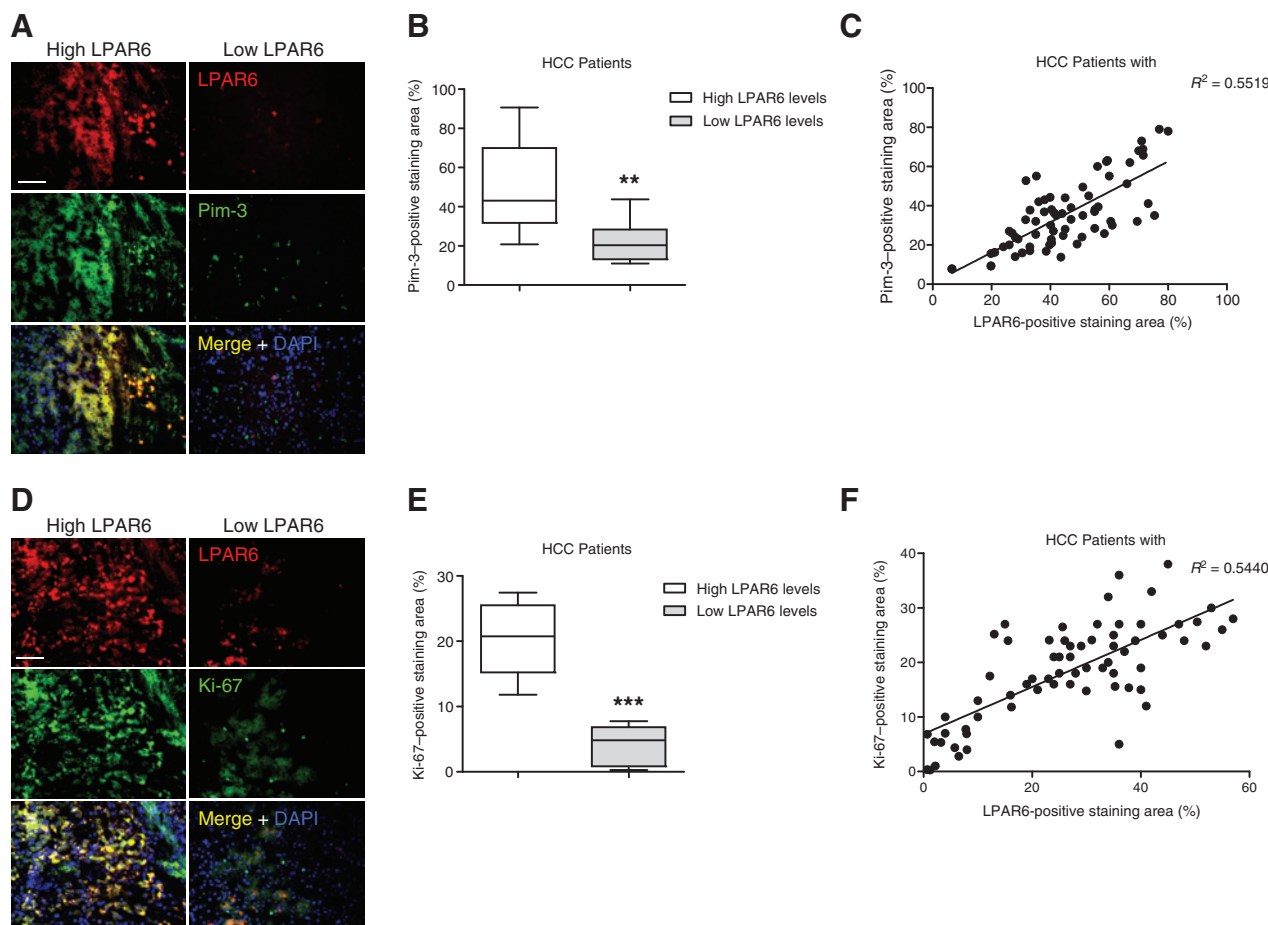## LPAR6 acts on the promoter and regulates the expression of the proto-oncogene *Pim-3*

To test the hypothesis that LPAR6 might be required for the transcriptional activation of proto-oncogene *Pim-3*, we investigated the effects of LPAR6, ectopically expressed in HLE cells, on the 5'-flanking region containing the promoter of the human *Pim-3* gene (Fig. 7A). To do so, we transiently transfected HLE-LPAR6 cells with a construct (pGL4.10) containing the luciferase reporter gene (*luc*) upstream of the entire promoter sequence of *Pim-3* (p2074-luc). This promoter sequence contains the binding sites of

Figure 5.

Pim-3 contributes to LPAR6-mediated growth and tumorigenicity in HCC; ectopic expression of *Pim-3* restores growth in LPAR6–knocked down cells, whereas downregulation of *Pim-3* decreases growth in LPAR6-overexpressing cells. A, significant downregulation of *Pim-3* mRNA expression levels in LPAR6–knocked down Huh7 cells compared with control-shRNA cells evaluated by real-time PCR (left) and Western blot (right). Error bars, SEM of three independent experiments, each conducted in triplicate. ***, $P < 0.001$. B, the *Pim-3* mRNA expression levels were similarly downregulated in tumors originated from nude mice injected with LPAR6-shRNA HuH7 cells compared with the control group (left). **, $P < 0.01$. The expression of protein kinase PIM3, evaluated by immunofluorescence, was significantly reduced in tumors from mice injected with LPAR6-shRNA#8HuH7 cells compared with controls (right). LPAR6 staining, PIM3, and merged images with DAPI staining for nuclei are shown. Scale bar, 100 μm. C, upregulation of *Pim-3* mRNA expression levels evaluated by real-time PCR (left) and Western blot (right) in HLE-LPAR6 compared with HLE-neo control cells and in nude mice intrasplenically inoculated with HLE-LPAR6 compared with control mice inoculated with HLE-neo. No *Pim-3* expression was detected in control mice. Error bars, SEM of three independent experiments, each conducted in triplicate. ***, $P < 0.001$. D, proliferation assay showing the restored cell growth in LPAR6-shRNA Huh7 cells ectopically expressing the PIM3-GFP vector. Treatment with the pharmacologic inhibitor of PIM3, SGI-1776 (5 μmol/L), blocked the contribution of *Pim-3* to cell growth. Error bars, SEM of three independent experiments. *, $P < 0.05$ vs. controls. E, proliferation assay showing that, in contrast, inhibition of *Pim-3* by both siRNAs and SGI-1776 reduces cell growth in HLE-LPAR6. Error bars, SEM of three independent experiments. *, $P < 0.05$; **, $P < 0.01$ vs. controls. F, proliferation assay validating the effect of *Pim-3*-siRNAs and SGI-1776 in a different HCC cell line overexpressing LPAR6 (PLC/PRF/5-LPAR6). Error bars, SEM of three independent experiments. **, $P < 0.01$ vs. controls.

several transcription factors, including STAT3, SP1, ETS1, and nuclear factor NF-κB. The results of the assay revealed that luciferase activity was present in HLE-LPAR6, whereas no activity was detected in HLE-neo control cells (Fig. 7B). Luciferase activity was also detectable in HLE-LPAR6 cells transfected with the deleted mutant p-809-luc (deletion between the position −2074 bp and −809 bp), which conserves the same binding sites as the p2074-luc vector (Fig. 7C). Conversely, decreased or no luciferase activity was observed in HLE-LPAR6 cells transfected with p264-luc (lacking the binding sites for STAT3) or p104-luc (no binding sites) vectors, respectively (Fig. 7B). Taken together, these data indicate that LPAR6 acts on the *Pim-3* gene promoter. Moreover, the use of deleted promoter sequences revealed that STAT3 is an important binding site for the activation of the proto-

oncogene *Pim-3* promoter. To corroborate this observation, we evaluated the luciferase activity of HLE-LPAR6 expressing the *Pim-3* promoter vector or the deleted mutants following STAT3 gene silencing by STAT3 siRNAs or treatment with STA-21 (30 μmol/L), a STAT3 selective inhibitor that inhibits the STAT3 binding to DNA (19). We found that both STAT3 siRNAs and STA-21 failed to increase luciferase activity in HLE-LPAR6 expressing the STAT3-binding sites (*p2074-luc and p809-luc*) compared with controls (HLE-LPAR6 control-siRNA and HLE-LPAR6 + vehicle; Fig. 7D). Figure 7E shows Western blot analysis demonstrating effective knockdown of STAT3 in HLE-LPAR6 expressing the pGL4 vectors harboring the entire *Pim-3* promoter fragment (*p2074-luc*) or the deleted mutants (*p809-luc, p264-luc, and p104-luc*). Together, these data demonstrate that the STAT3-DNA binding site on
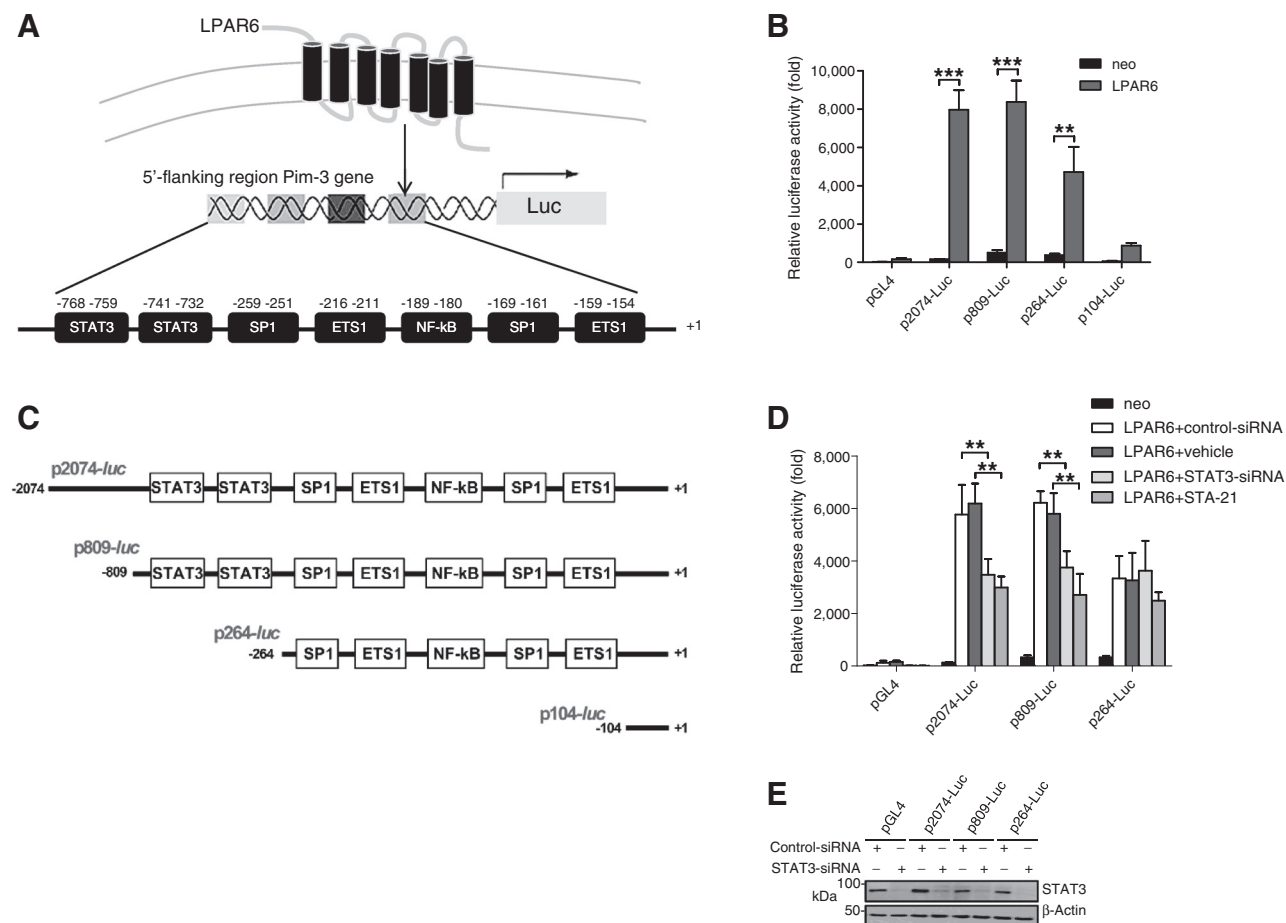
Figure 6.
LPAR6 expression levels are correlated with *Pim-3* and the Ki-67 proliferative index in patients with HCC. A, correlation between the expression of *Pim-3* and LPAR6 in patients with HCC. Patients' tissues were stratified and scored according to the intensity of LPAR6 staining (red) as high ($n = 37$) and low ($n = 33$) expression levels, and representative immunofluorescence images of LPAR6 staining (red), PIM3 (green), and merged images (yellow) with DAPI staining (blue) for nuclei are shown. Scale bar, 100 μm. B, box and whisker plot showing elevated expression of PIM3 in HCC tissues with high levels of LPAR6 and reduced PIM3 expression in HCC tissues expressing low levels of LPAR6. **, $P < 0.01$. C, Pearson scatterplot showing the correlation between LPAR6 and PIM3 expression levels in tissues from patients with HCC. A significant correlation was found between LPAR6- and PIM3-positive stained areas ($P < 0.0001$; R = 0.55). D, correlation between LPAR6 and Ki-67 expression levels in patients with HCC; representative immunofluorescence images reporting LPAR6 (red) and Ki-67 (green) staining and merged images (yellow) with DAPI staining (blue) for nuclei are shown. Scale bar, 100 μm. E, box and whisker plot displaying comparison between LPAR6 and Ki-67 expression levels in HCC. ***, $P < 0.001$. F, Pearson scatterplot showing the correlation between LPAR6 and Ki-67 expression levels in tissues of patients with HCC. A significant correlation was found between LPAR6- and Ki-67–positive stained areas ($P < 0.0001$; R = 0.54).

the *Pim-3* promoter is indeed relevant for the activation of *Pim-3* by LPAR6.

Discussion

Our current study reveals novel findings concerning the pathogenic role of LPAR6 in liver cancer and shows that LPAR6 functions as a promoter of tumorigenicity of HCC via the transcriptional activation of several genes, including *Pim-3*. This highlights the role of the LPA axis in HCC. We have previously demonstrated that LPA promotes HCC progression by stimulating the recruitment and transdifferentiation of peritumoral fibroblasts into carcinoma-associated fibroblasts (17). Here, we used a gain- and loss-of-function approach to elucidate how LPAR6 sustains the HCC tumorigenic process. In addition, we employed deletion mutants to corroborate the involvement of LPAR6 in this process. We also performed an extensive gene profiling analysis by

Massive Analysis of cDNA Ends (MACE) to gain insight into genes under the control of LPAR6. Lastly, we show that data obtained in patients on the involvement of LPAR6 in HCC progression, as well as on the existing cross-talk between LPAR6 and *Pim-3*, are consistent with the experimental data. A descriptive study by Sokolov and colleagues (20) recently reported increased expression levels of LPAR6 in HCC. Our findings have extended these observations, disclosing a disease mechanism and attributing to LPAR6 a potential role as a biomarker predicting clinical outcome in patients with HCC. This is corroborated by the findings that LPAR6 levels are correlated with overall survival in patients with HCC, and that patients with high levels of LPAR6 have a poor prognosis. In our patient analysis, LPAR6 score seems to correlate with tumor size, so poor outcome could be expected. However, because LPAR6 sustains tumor growth and tumorigenicity giving the cancer cell a proliferative advantage over its neighbors, it is likely that larger tumors contain more LPAR6-expressing cells. In

Mazzocca et al.

Figure 7.
The proto-oncogene *Pim-3* is under the transcriptional control of LPAR6 in HCC. A, schematic illustration showing the binding sites for STAT3, SP1, ETS1, and NF-κB transcription factors in the 5′-flanking region between −768 and −154 bp of the promoter of the human *Pim-3* gene. This promoter region was cloned into a pGL4.10 (luc2) firefly luciferase reporter gene vector. B, luciferase activities of HLE-neo and HLE-LPAR6 transfected with pGL4 vectors containing the entire *Pim-3* promoter fragment (*p2074-luc*) or deleted mutants (*p809-luc*, *p264-luc*, and *p104-luc*) or pGL4.10 luciferase empty vector as control. Error bars, SEM of three independent experiments, each conducted in triplicate. **, $P < 0.01$; ***, $P < 0.001$, HLE-LPAR6 vs. HLE-neo. C, detailed illustration of the entire 5′-flanking region of the promoter of the human *Pim-3* gene (*p2074-luc*) and the deleted mutants (*p809-luc*, *p264-luc*, and *p104-luc*) cloned into the pGL4.10 firefly luciferase reporter gene vector and used for experiments. D, effect of STAT3-siRNAs and STA-21 (30 μmol/L), a STAT3 selective inhibitor, on the luciferase activities of HLE-neo and HLE-LPAR6 transfected with pGL4 vectors containing the entire *Pim-3* promoter fragment (*p2074-luc*) or deleted mutants (*p809-luc*, *p264-luc*, and *p104-luc*) or pGL4.10 luciferase empty vector as control. Error bars, SEM of three independent experiments, each conducted in triplicate. **, $P < 0.05$ STAT3-silenced HLE-LPAR6 or STA-21–treated HLE-LPAR6 vs. control-siRNA or vehicle, respectively. E, Western blot showing the effect of STAT3 silencing in HLE-LPAR6 transfected with pGL4.10 vector alone (control) or containing the entire *Pim-3* promoter fragment (*p2074-luc*) or deleted mutants (*p809-luc*, *p264-luc*, and *p104-luc*).

addition, we show the importance of LPAR6 expression in HCC regardless of circulating LPA levels. Blood LPA levels may vary in patients with HCC, although they are generally elevated compared with cirrhotic and healthy donors (17). This supports the idea that both elevated circulating LPA concentrations and LPAR6 tumor levels are important contributors to human disease.

Of similar importance is our finding demonstrating the role of LPAR6 in maintaining the tumorigenic potential of cancer cells. A possible explanation for this striking effect could be that LPAR6 orchestrates the function of multiple genes, as shown by our MACE experiments. Aberrant LPAR6 expression dysregulates genes involved in fundamental biologic processes, including tissue development, lipid metabolism and cytoskeleton, and ECM organization, and this may explain the tumorigenic activity in cancer cells. When LPAR6 is ectopically expressed, the growth potential is significantly increased, in an anchorage-independent

manner, this being a typical hallmark of tumorigenicity. Our results suggest that the C-terminal domains of LPAR6 protein are involved in exerting this effect, because truncated LPAR6 mutants failed to promote tumor growth in our model. Interestingly, these mutants are responsible for lack of hair follicle growth and the generation of a genetic form of alopecia called hypotrichosis simplex (15). It is likely that a molecular mechanism involved in hair growth could be dysregulated during cancer growth and that the C-terminal portion of LPAR6 could be functionally implicated.

Digital expression profiling shows that genes with an altered expression as a consequence of LPAR6 knockdown are genes known to participate in the tumorigenic process. Among these, connective tissue growth factor (CTGF), FGFR1, ITGA2, BRCA2, and PIM3 were significantly downregulated. The involvement of CTGF in cancer and in particular in HCC is documented

(21–23). Our gene profiling data also reveal alterations in genes controlling lipid metabolism and homeostasis, suggesting the existence of a molecular cross-talk between LPA and other lipid pathways. Moreover, genes involved in ECM organization such as *MMP19*, *ITGA6*, and several collagen genes were significantly downregulated. It is noteworthy that the *ITGA6* gene encoding integrin α6 plays a role in the tumorigenic process of many cancers including HCC (24, 25). Among genes that control tissue development, we focused on *Pim-3* because, being an oncogene, it could largely explain the LPAR6-mediated protumorigenic phenotype observed in HCC. Indeed, we have demonstrated that LPAR6 acts on the promoter and finely regulates the expression of *Pim-3*. This is consistent with the fact that *Pim-3* is downregulated in LPAR6-shRNA cells and upregulated in LPAR6-overexpressing cells, and with the observation that *Pim-3* expression is increased in patients with HCC overexpressing LPAR6. Whether *Pim-3* is a predictor of clinical outcome and survival of patient with HCC was not an issue addressed in our study. Nevertheless, Zheng and colleagues (26) have suggested that *Pim-3* may be useful to predict the prognosis of patients with gastric cancer. In terms of gene regulation, our findings clearly demonstrate that the LPAR6 signaling axis activates the transcription of *Pim-3* by acting on the gene promoter that contains the binding sites for several transcription factors, including STAT3, SP1, ETS1, and nuclear factor NF-κB. Although the role of LPA in inducing NF-κB activation has been described (27), no report has yet shown the activation of STAT3 by LPA. Our results suggest that the STAT3-binding site is important for the activation of *Pim-3* by LPAR6 because experiments using the deleted mutant *p264*, lacking the binding sites for STAT3, show a significantly decreased luciferase activity.

In conclusion, we provide evidence that LPAR6 is essential to maintain the tumorigenic properties of cancer cells, and that this occurs through the regulation of multiple genes including proto-oncogene *Pim-3*. Both experimental evidence and patients data reported in this study support the role of LPAR6 as a driver of tumorigenicity and growth in HCC. Future studies will evaluate the genetic and epigenetic factors that act on the LPAR6 signaling axis during the tumorigenic process, and whether these factors affect the LPAR6 gene in HCC precan-cerous conditions such as liver cirrhosis and dysplastic nodules. Moreover, it will be important to determine whether changes in LPAR6 expression or downstream signaling effectors are critical in different types of cancers other than HCC, and if they are predictive of patient survival. Lastly, this study provides a preclinical rationale for therapeutic targeting of LPAR6-*Pim-3* in HCC.

Disclosure of Potential Conflicts of Interest

No potential conflicts of interest were disclosed.

Authors' Contributions

Conception and design: A. Mazzocca
Development of methodology: A. Mazzocca, F. De Santis, N. Mukaida
Acquisition of data (provided animals, acquired and managed patients, provided facilities, etc.): A. Mazzocca, R.C. Betz
Analysis and interpretation of data (e.g., statistical analysis, biostatistics, computational analysis): A. Mazzocca, A. Filannino, N. Mukaida
Writing, review, and/or revision of the manuscript: A. Mazzocca
Administrative, technical, or material support (i.e., reporting or organizing data, constructing databases): A. Mazzocca, Y.-Y. Li
Study supervision: A. Mazzocca
Other (performed experiments): F. Dituri, A. Filannino, C. Lopane
Other (helped with discussion and comments on the project): C. Tortorella, C. Sabbà

References

1. Parkin DM, Bray F, Ferlay J, Pisani P. Global cancer statistics, 2002. CA Cancer J Clin 2005;55:74–108.
2. Mittal S, El-Serag HB. Epidemiology of hepatocellular carcinoma: consider the population. J Clin Gastroenterol 2013;47 Suppl:S2–6.
3. Naugler WE, Sakurai T, Kim S, Maeda S, Kim K, Elsharkawy AM, et al. Gender disparity in liver cancer due to sex differences in MyD88-dependent IL-6 production. Science 2007;317:121–4.
4. Siegel AB, Zhu AX. Metabolic syndrome and hepatocellular carcinoma: two growing epidemics with a potential link. Cancer 2009;115:5651–61.
5. Farazi PA, DePinho RA. Hepatocellular carcinoma pathogenesis: from genes to environment. Nat Rev Cancer 2006;6:674–87.
6. Giannelli G, Antonaci S. Novel concepts in hepatocellular carcinoma: from molecular research to clinical practice. J Clin Gastroenterol 2006; 40:842–6.
7. Yang JD, Nakamura I, Roberts LR. The tumor microenvironment in hepatocellular carcinoma: current status and therapeutic targets. Semin Cancer Biol 2011;21:35–43.
8. Zhu AX, Duda DG, Sahani DV, Jain RK. HCC and angiogenesis: possible targets and future directions. Nat Rev Clin Oncol 2011;8:292–301.
9. Mazzocca A, Liotta F, Carloni V. Tetraspanin CD81-regulated cell motility plays a critical role in intrahepatic metastasis of hepatocellular carcinoma. Gastroenterology 2008;135:244–56 e1.
10. Mitsunobu M, Toyosaka A, Oriyama T, Okamoto E, Nakao N. Intrahepatic metastases in hepatocellular carcinoma: the role of the portal vein as an efferent vessel. Clin Exp Metastasis 1996;14:520–9.
11. Mills GB, Moolenaar WH. The emerging role of lysophosphatidic acid in cancer. Nat Rev Cancer 2003;3:582–91.
12. van Corven EJ, Groenink A, Jalink K, Eichholtz T, Moolenaar WH. Lysophosphatidate-induced cell proliferation: identification and dissection of signaling pathways mediated by G proteins. Cell 1989;59:45–54.
13. Moolenaar WH, van Meeteren LA, Giepmans BN. The ins and outs of lysophosphatidic acid signaling. Bioessays 2004;26:870–81.
14. Choi JW, Herr DR, Noguchi K, Yung YC, Lee CW, Mutoh T, et al. LPA receptors: subtypes and biological actions. Annu Rev Pharmacol Toxicol 2010;50:157–86.
15. Pasternack SM, von Kugelgen I, Al Aboud K, Lee YA, Ruschendorf F, Voss K, et al. G protein-coupled receptor P2Y5 and its ligand LPA are involved in maintenance of human hair growth. Nat Genet 2008;40:329–34.

16. Shimomura Y, Wajid M, Ishii Y, Shapiro L, Petukhova L, Gordon D, et al. Disruption of P2RY5, an orphan G protein-coupled receptor, underlies autosomal recessive woolly hair. Nat Genet 2008;40:335–9.

17. Mazzocca A, Dituri F, Lupo L, Quaranta M, Antonaci S, Giannelli G. Tumor-secreted lysophostatidic acid accelerates hepatocellular carcinoma progression by promoting differentiation of peritumoral fibroblasts in myofibroblasts. Hepatology 2011;54:920–30.

18. Li YY, Wu Y, Tsuneyama K, Baba T, Mukaida N. Essential contribution of Ets-1 to constitutive Pim-3 expression in human pancreatic cancer cells. Cancer Sci 2009;100:396–404.

19. Song H, Wang R, Wang S, Lin J. A low-molecular-weight compound discovered through virtual database screening inhibits Stat3 function in breast cancer cells. Proc Natl Acad Sci U S A 2005;102:4700–5.

20. Sokolov E, Eheim AL, Ahrens WA, Walling TL, Swet JH, McMillan MT, et al. Lysophosphatidic acid receptor expression and function in human hepatocellular carcinoma. J Surg Res 2013;180:104–13.

21. Chu CY, Chang CC, Prakash E, Kuo ML. Connective tissue growth factor (CTGF) and cancer progression. J Biomed Sci 2008;15:675–85.

22. Urtasun R, Latasa MU, Demartis MI, Balzani S, Goni S, Garcia-Irigoyen O, et al. Connective tissue growth factor autocriny in human hepatocellular carcinoma: oncogenic role and regulation by epidermal growth factor receptor/yes-associated protein-mediated activation. Hepatology 2011; 54:2149–58.

23. Mazzocca A, Fransvea E, Dituri F, Lupo L, Antonaci S, Giannelli G. Down-regulation of connective tissue growth factor by inhibition of transforming growth factor beta blocks the tumor-stroma cross-talk and tumor progression in hepatocellular carcinoma. Hepatology 2010;51: 523–34.

24. Rabinovitz I, Mercurio AM. The integrin alpha 6 beta 4 and the biology of carcinoma. Biochem Cell Biol 1996;74:811–21.

25. Carloni V, Mazzocca A, Pantaleo P, Cordella C, Laffi G, Gentilini P. The integrin, alpha6beta1, is necessary for the matrix-dependent activation of FAK and MAP kinase and the migration of human hepatocarcinoma cells. Hepatology 2001;34:42–9.

26. Zheng HC, Tsuneyama K, Takahashi H, Miwa S, Sugiyama T, Popivanova BK, et al. Aberrant Pim-3 expression is involved in gastric adenoma-adenocarcinoma sequence and cancer progression. J Cancer Res Clin Oncol 2008;134:481–8.

27. Sun W, Yang J. Molecular basis of lysophosphatidic acid-induced NF-kappaB activation. Cell Signal 2010;22:1799–803.

Cancer Research

AACR

Lysophosphatidic Acid Receptor LPAR6 Supports the Tumorigenicity of Hepatocellular Carcinoma

Antonio Mazzocca, Francesco Dituri, Flavia De Santis, et al.

Updated version	Access the most recent version of this article at: doi:10.1158/0008-5472.CAN-14-1607

E-mail alerts	Sign up to receive free email-alerts related to this article or journal.
Reprints and Subscriptions	To order reprints of this article or to subscribe to the journal, contact the AACR Publications Department at pubs@aacr.org.
Permissions	To request permission to re-use all or part of this article, contact the AACR Publications Department at permissions@aacr.org.